Magnetic phase diagrams of $MnWO_4$

1997 J. Phys.: Condens. Matter 9 3189

(http://iopscience.iop.org/0953-8984/9/15/011)

J. Phys.: Condens. Matter **9** (1997) 3189–3203. Printed in the UK PII: S0953-8984(97)80083-5

Magnetic phase diagrams of $MnWO_4$

H Ehrenberg†, H Weitzel†, C Heid†, H Fuess†, G Wltschek‡, T Kroener§, J van Tol‖ and M Bonnet¶

† Fachbereich Materialwissenschaft, Fachgebiet Strukturforschung, Technische Hochschule Darmstadt, D-64287 Darmstadt, Germany

‡ Interdisciplinary Research Centre in Superconductivity, University of Cambridge, Madingley Road, Cambridge CB3 0HE, UK

§ Forschungszentrum Karlsruhe, Institut für Technische Physik, POB 3640, D-76021 Karlsruhe, Germany

‖ Grenoble High Magnetic Field Laboratory, MPI-F/CNRS, BP 166, F-38042 Grenoble Cédex 9, France

¶ Centre d'Etudes Nucléaires de Grenoble, F-38041 Grenoble, France

Received 4 December 1996

Abstract. For the compound $MnWO_4$ of wolframite structure three antiferromagnetic phases are known to exist in the absence of an external field. In this contribution we present the magnetic phase diagrams up to a field strength of 20 T. The plane spanned by the easy direction and the orientation of the twofold screw axes is exposed for the application of external magnetic fields, and the change in the topology of the phase diagrams with the variation of the specific field direction within this plane is described in detail. The application of an external magnetic field perpendicular to this plane hardly affects the stability ranges of any of the phases.

1. Introduction

The wolframite structure of $MnWO_4$ is based on a hexagonal close packing of oxygen ions with half of the octahedral interstices filled by cations. The Mn and W ions are distributed in alternating layers perpendicular to the a-axis, if the standard setting, $P2/c$ and $\beta > 90^\circ$, is used [1]. Within these layers the filled oxygen octahedra are interconnected by common edges, and therefore zigzag chains result. In a previous article three magnetic phase transitions have been reported for $MnWO_4$ without an external magnetic field applied [1]. Accordingly the collinear magnetic structure of the AF3 phase is stable in the temperature range $12.3\ \mathrm{K} < T < 13.5\ \mathrm{K}$ and exhibits a sinusoidal modulation of the ordered magnetic moments. The easy direction lies in the ac-plane forming an angle of 35° with the $+a$-direction in the $+a+c$-quadrant. Accompanied with a second-order phase transition, an additional component of the ordered magnetic moment in the [010] direction arises in the AF2 phase, increasing continuously with decreasing temperature, and therefore a coplanar and elliptically modulated magnetic structure results. For various samples and by different techniques a first-order phase transition AF1 $\leftrightarrow$ AF2 is observed between 6.8 K and 8.0 K. The magnetic structure of the ground state AF1 is collinear again, with the ordered moments aligned in the same direction as in the AF3 phase, hereafter called the easy direction. The translational symmetry of phases AF2 and AF3 is described by the same propagation vector $\boldsymbol{k}$, which is different to that for the AF1 phase. $MnWO_4$ is an interesting and promising model compound for the investigation of critical phenomena and the simulation of phase

0953-8984/97/153189+15$19.50

diagrams: on the one hand at least three magnetically ordered phases exist, with both temperature- and field-induced transitions between them; on the other hand the crystal structure is rather simple and all of the Mn ions are situated at one crystallographic site of twofold rotational symmetry. Therefore, the investigation of magnetism in $MnWO_4$ has been extended, and in this contribution we present the magnetic phase diagrams of $MnWO_4$ for several field directions, and field strengths up to 12 T and 20 T, respectively. In section 2 we premise an investigation of the profiles of magnetic satellites to obtain more precise values for the components k_x and k_z of the propagation vectors in the AF2 and AF3 phases. They cannot be expressed as ratios of small integer numbers, and a reliable estimation of the experimental errors is lacking in previous work [1]. The experimental methods applied for the determination of the magnetic phase diagrams are sketched in section 3; also given is a description of the parametrizations used for fixing the specific phase boundaries. Section 4 presents the observed magnetic phase diagrams.

Table 1. Results of the quantitative analysis of the profile studies. N is the number of points included with at least 75% of the maximum intensity, which have been used for the calculation of the peak centre and the estimation of the error.

T (K)	h	k	l	I_{max}	N	Monitor
5.5	−0.2497(30)	$-\frac{1}{2}$	1.4978(60)	1824	73	160 000
5.5	−0.7441(61)	$-\frac{1}{2}$	0.4969(38)	3941	45	160 000
5.5	−0.7464(44)	$-\frac{1}{2}$	1.4971(58)	836	120	160 000
9.0	−0.2164(25)	$-\frac{1}{2}$	1.4553(59)	752	66	80 000
9.0	−0.7757(59)	$-\frac{1}{2}$	0.5394(40)	2606	44	160 000
9.0	−0.7812(48)	$-\frac{1}{2}$	1.5411(63)	664	93	160 000
11.5	−0.2162(28)	$-\frac{1}{2}$	1.4557(62)	998	66	160 000
11.5	−0.7759(55)	$-\frac{1}{2}$	0.5394(40)	1802	41	160 000
11.5	−0.7817(51)	$-\frac{1}{2}$	1.5417(60)	528	88	160 000
12.9	−0.2140(30)	$-\frac{1}{2}$	1.4545(68)	539	70	160 000
12.9	−0.7776(61)	$-\frac{1}{2}$	0.5403(44)	934	53	160 000
9.0	−0.9966(49)	0	2.0004(48)	7271	53	40 000
9.0	0.0020(25)	0	1.9988(61)	1617	42	40 000
9.0	−0.0020(21)	−1	0.9938(72)	2106	42	40 000
9.0	−0.9984(58)	−1	1.9946(56)	350	68	80 000

2. Profile analysis of magnetic satellites

By means of high-resolution neutron powder diffraction very precise values for the d-spacings can be achieved, but the derived values [1, 2] for the components $k_x = -0.214$ and $k_z = 0.457$ of the propagation vectors in the AF2 and AF3 phases are less accurate than in single-crystal studies, because of the strong correlation between the two components in monoclinic systems and the large uncertainty arising from the decoupling procedure. The component k_y is definitely equal to $\frac{1}{2}$ for all antiferromagnetic phases. We have investigated

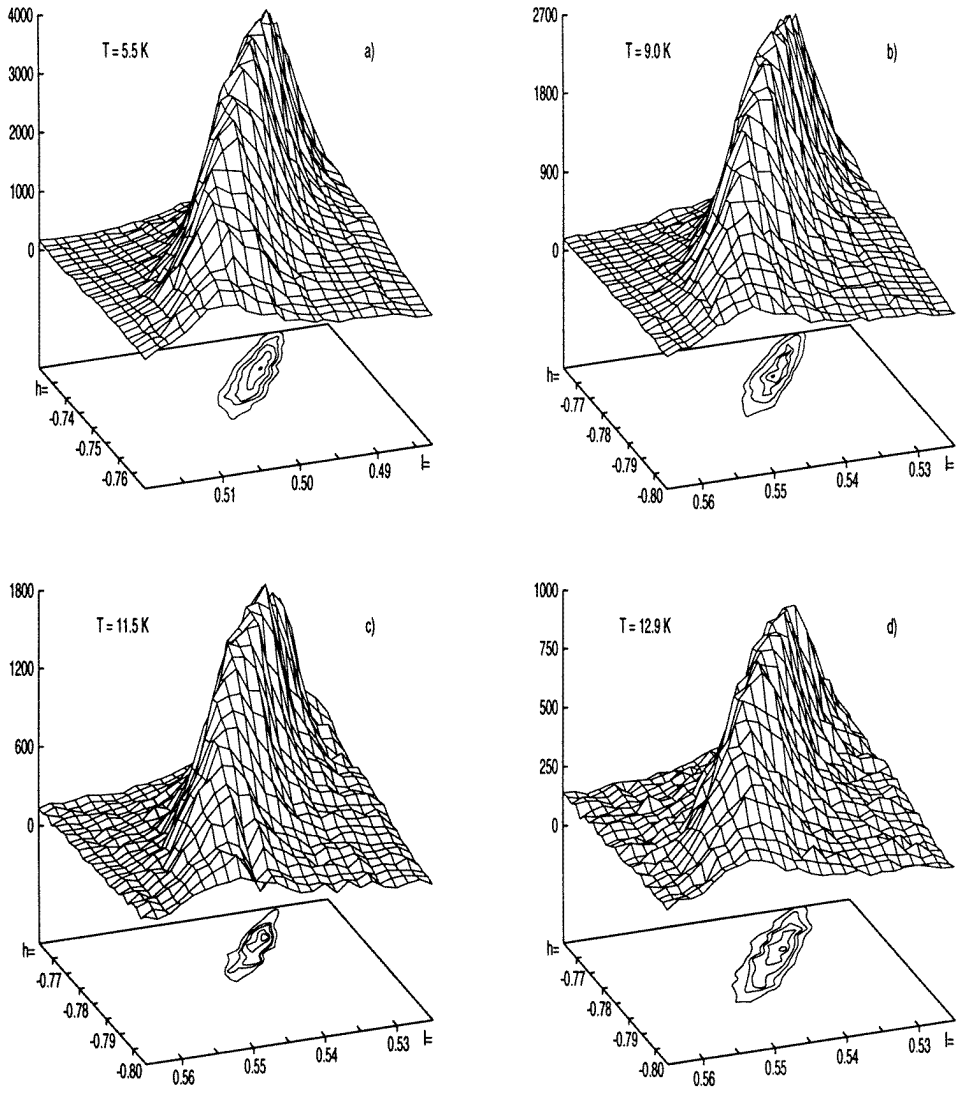

Figure 1. Profiles of the magnetic satellites $(-1\ 0\ 1)^-$ at different temperatures: (a) 5.5 K (AF1), (b) 9.0 K, (c) 11.5 K (AF2) and (d) 12.9 K (AF3).

the profiles of magnetic satellites by single-crystal neutron diffraction for all of the phases, AF1, AF2 and AF3, as well as the profiles of some nuclear reflections for the sake of comparison, using the instrument DN4 at the SILOË reactor of the CENG, France. In figure 1 the profiles are shown for the satellites $(-1\ 0\ 1)^-$ as representatives. Note that another section of the *hl*-plane is shown for the phase AF1 as compared to the other phases. All of the profiles are similar, including those of nuclear reflections in the neighbourhood of the magnetic satellites in reciprocal space, so domain size effects are not expected to influence the profiles significantly. For the determination of the peak positions all of the points with at least 75% of the maximum intensity were included for the calculation of the

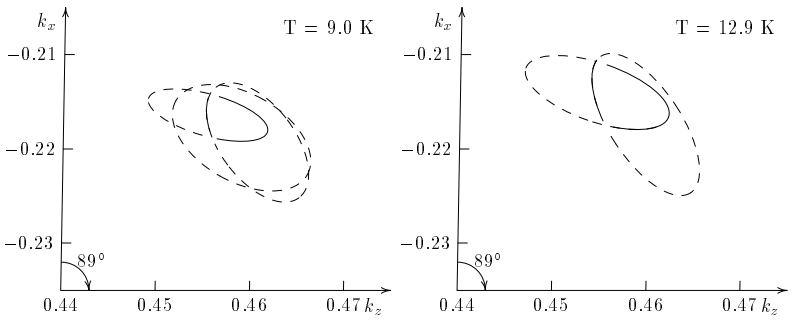

Figure 2. Projections of the resolution ellipsoids in the k_x–k_z-plane as used for the determination of the propagation vectors in the AF2 and AF3 phases.

centres and corresponding standard deviations, each point weighted with its intensity; see table 1. This procedure and the choice of the intensity criterion of 75% are justified by the reasonable values for the nuclear reflections. The orientation of the resolution ellipsoids in the *hl*-plane can be derived from the contour lines as shown in figure 1. Combining the results for different satellites, the following values and estimated errors are derived, as sketched in figure 2:

$$\text{AF1}: \begin{cases} k_x = -\dfrac{1}{4} \\ k_y = \dfrac{1}{2} \\ k_z = \dfrac{1}{2} \end{cases} \qquad \text{AF2}: \begin{cases} k_x = -0.2165(25) \\ k_y = \dfrac{1}{2} \\ k_z = 0.4585(25) \end{cases} \qquad \text{AF3}: \begin{cases} k_x = -0.2145(30) \\ k_y = \dfrac{1}{2} \\ k_z = 0.4580(35). \end{cases} \tag{1}$$

3. Experimental details and the procedure of the analysis

To determine the dependence of the phase boundaries on the direction of the external field, both magnetization and specific heat measurements in an applied field have been performed. For the latter a semi-adiabatic heat pulse calorimeter was used with an external-field option up to 9 T described elsewhere [3]. In order to acquire a specific field direction, the crystal was mounted on an individually cut wedge of sapphire. For the magnetization measurements three different instruments have been used, depending on the required field strength. Up to 5.5 T the experiments were carried out with a superconducting quantum interference device (Quantum Design), for higher fields up to 12 T with a vibrating-sample magnetometer (Oxford Instruments), and for fields up to 20 T with an extraction magnetometer in a resistive magnet at the Grenoble High Magnetic Field Laboratory .

The phase transition AF1 → AF2 is of first order and is therefore accompanied by a jump in the temperature dependence of the magnetization at constant field strength, while the transitions AF2 → AF3 and AF3 → the paramagnetic region P are of second order, and at the transition temperatures bends in the magnetization curve occur. The following parametrization has been used to determine both the transition temperature and the jump in

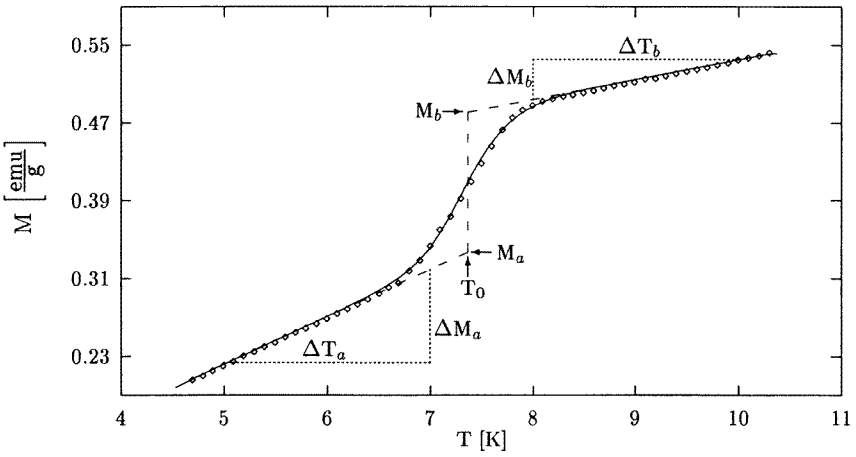

Figure 3. The parametrization of the magnetization in temperature scans at constant field strength as used for the determination of the transition temperature T_0 and the jump in magnetization $\Delta M = M_b - M_a$. The data were obtained with a superconducting quantum interference device shown for a field strength of $H = 0.4$ T and the field applied along the easy direction as representatives. The line indicates the curve calculated according to (2).

magnetization for the first-order transitions:

$$\begin{aligned} M(T) &= M_1(T) + M_2(T) \\ M_1(T) &= \begin{cases} \dfrac{\Delta M_a}{\Delta T_a}(T - T_0) + M_a & T < T_0 \\ \dfrac{\Delta M_b}{\Delta T_b}(T - T_0) + M_b & T \geqslant T_0 \end{cases} \\ M_2(H) &= \frac{1}{2}(M_b - M_a)\tanh[\sigma(T - T_0)]. \end{aligned} \tag{2}$$

The meanings of these parameters are illustrated in figure 3 for a typical experiment in the temperature range of a first-order phase transition. The transitions of second order are accompanied with bends in the magnetization, and the transition temperatures are derived by fitting continuously connected straight lines of different slopes to the experimental data.

The field-induced phase transitions of first order exhibit a pronounced hysteresis in the dependence of the magnetization on the field strength. To obtain an objective criterion for the phase boundary, the derivative $\Delta M/\Delta H$ of the magnetization M with respect to the field strength H was computed numerically, and the following parametrization:

$$\begin{aligned} \frac{\Delta M}{\Delta H}(H) &= \Delta M_1(H) + \Delta M_2(H) \\ \Delta M_1(H) &= \begin{cases} a & H < H_0 - 2\sigma \\ a + \dfrac{b-a}{4\sigma}(H - H_0 + 2\sigma) & H_0 - 2\sigma \leqslant H_0 + 2\sigma \\ b & H > H_0 + 2\sigma \end{cases} \\ \Delta M_2(H) &= c\exp\left[-\frac{(H - H_0)^2}{\sigma^2}\right] \end{aligned} \tag{3}$$

with refinable parameters a, b, c, σ and H_0 is fitted to the experimental data for the cases of increasing ($\Delta H > 0$) and decreasing ($\Delta H < 0$) fields. The phase transition field strength was defined to be the average of the maxima for $\Delta H > 0$ and $\Delta H < 0$ with an uncertainty of either half the difference between these maxima or the parameter σ. The maxima of both values are shown in the following diagrams as vertical error bars.

4. The magnetic phase diagrams

The magnetic structure of the ground state AF1 is collinear, and therefore the direction of the magnetic moments in zero field, the so-called easy direction, is exposed with respect to the orientation of an external magnetic field.

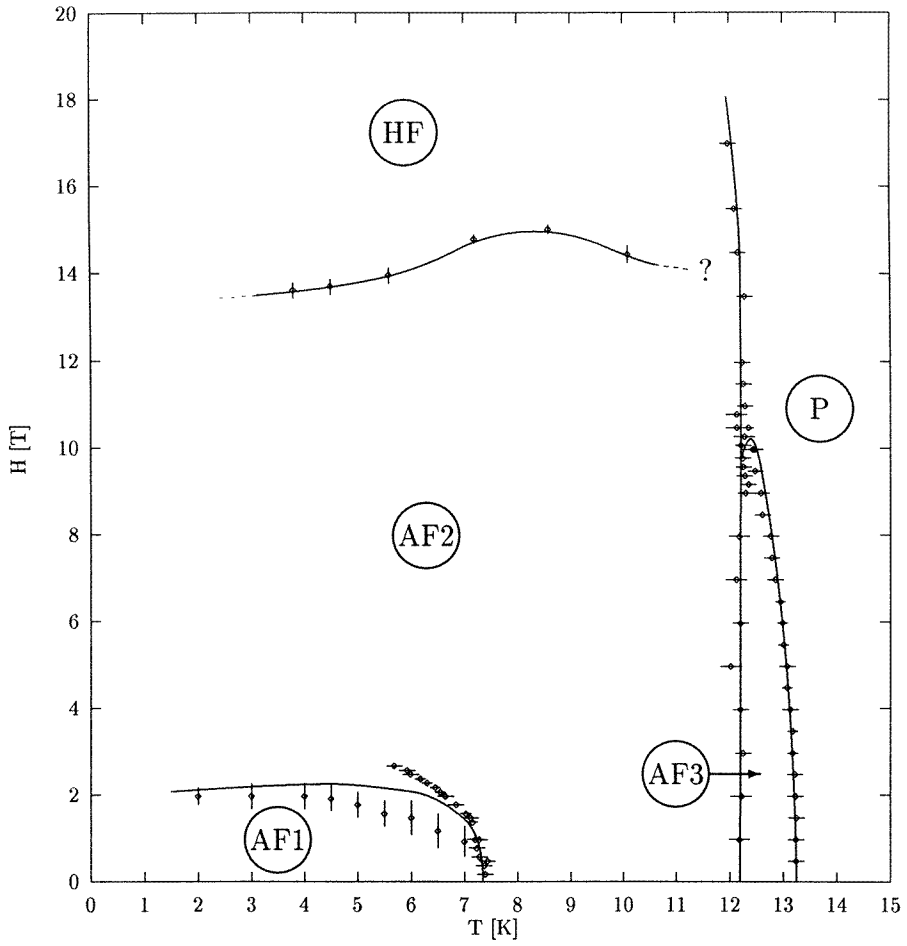

Figure 4. The magnetic phase diagram of $MnWO_4$ for an applied field parallel to the easy direction.

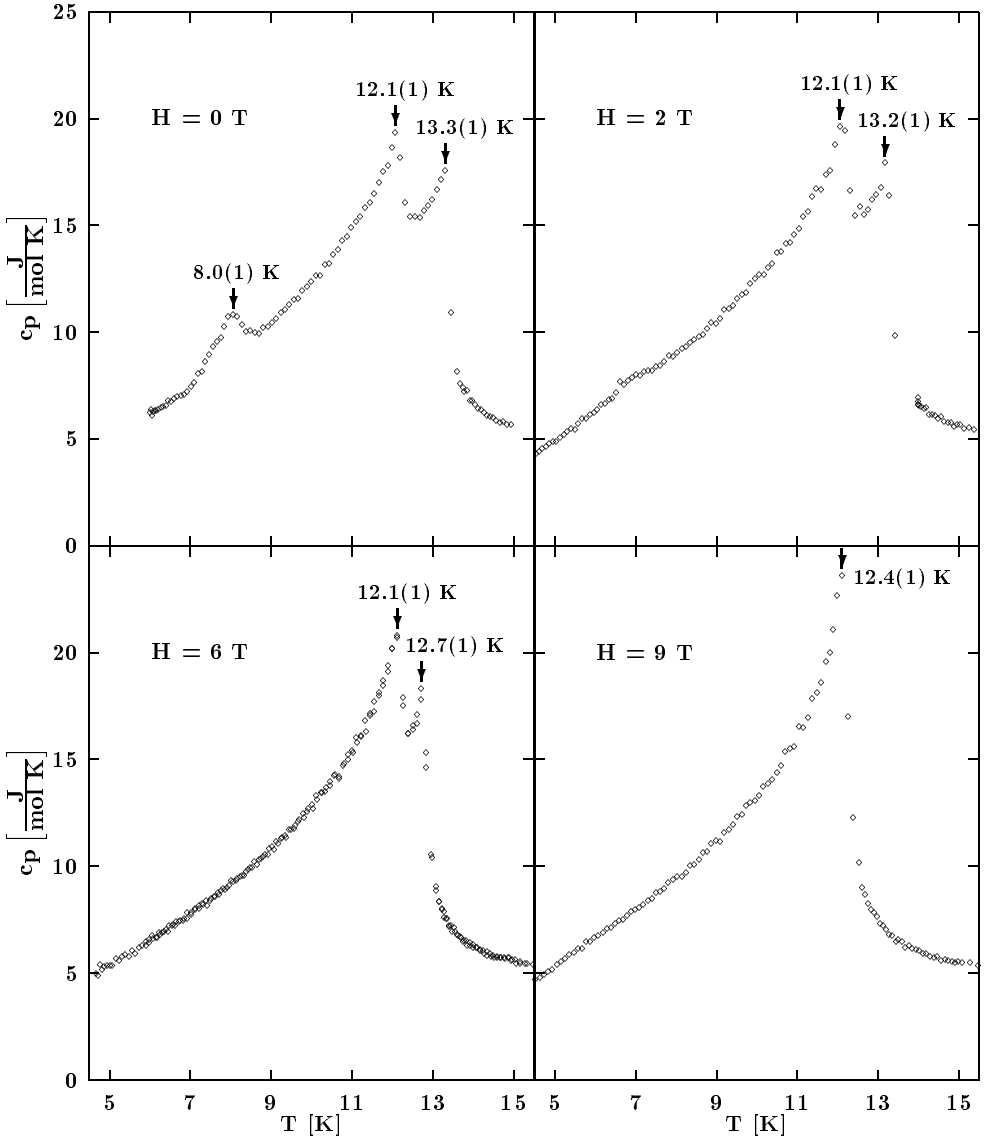

Figure 5. The specific heat of $MnWO_4$ in an external magnetic field parallel to the easy direction: $H = 0$ T, $H = 2$ T, $H = 6$ T and $H = 9$ T.

4.1. The easy direction

The magnetic phase diagram for this field direction is shown in figure 4 for field strength up to 20 T. A field strength of $H > 2$ T is sufficient to stabilize the intermediate phase AF2 to the lowest temperatures examined; it induces a phase transition from AF1 to AF2 at constant temperature with pronounced hysteresis effects. A further increase in field strength reduces the stability range of the AF3 phase up to $H = 9$ T, where the AF3 phase has vanished. This is readily derived from the specific heat measurements with a field applied along the easy direction; see figure 5. The existence of a new high-field phase (HF) at

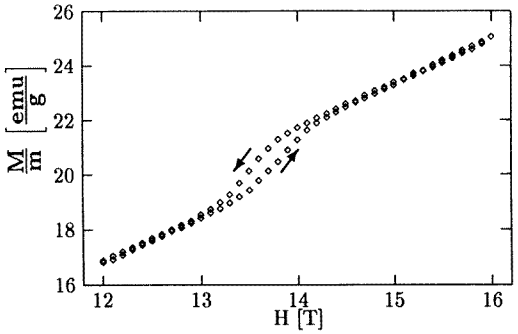

Figure 6. The field dependence of the magnetization in the range of the field-induced phase transition AF2 ↔ HF at $T = 3.8$ K for increasing and decreasing fields parallel to the easy direction.

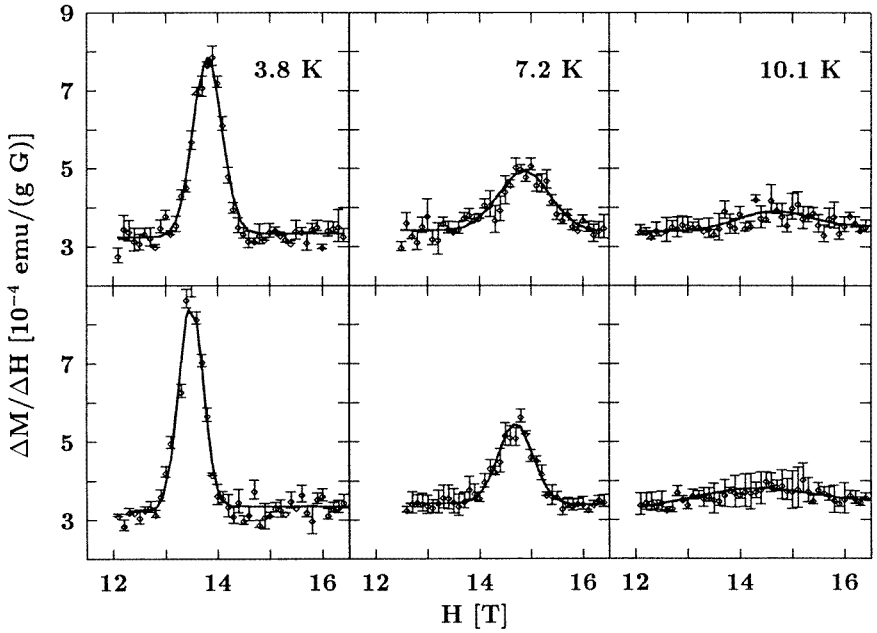

Figure 7. The field dependence of $\Delta M/\Delta H$ in the range of field-induced phase transitions AF2 ↔ HF at different temperatures for increasing (top line) and decreasing fields (bottom line) parallel to the easy direction.

$H \sim 14$ T is manifested in the field dependence of the magnetization as shown in figure 6 for $T = 3.8$ K. The first-order phase boundary is drawn according to section 3, and the effect of the thermal wash-out of this transition is indicated in figure 7. Therefore the detailed course of this phase boundary near to the paramagnetic region could not have been determined by this method, as indicated by the question mark in figure 4.

All of the phase transitions are reflected in the temperature dependence of the magnetization at constant field strength, so these experimental results are of particular interest and are therefore shown; see figure 8. At field strength $H < 2$ T and low

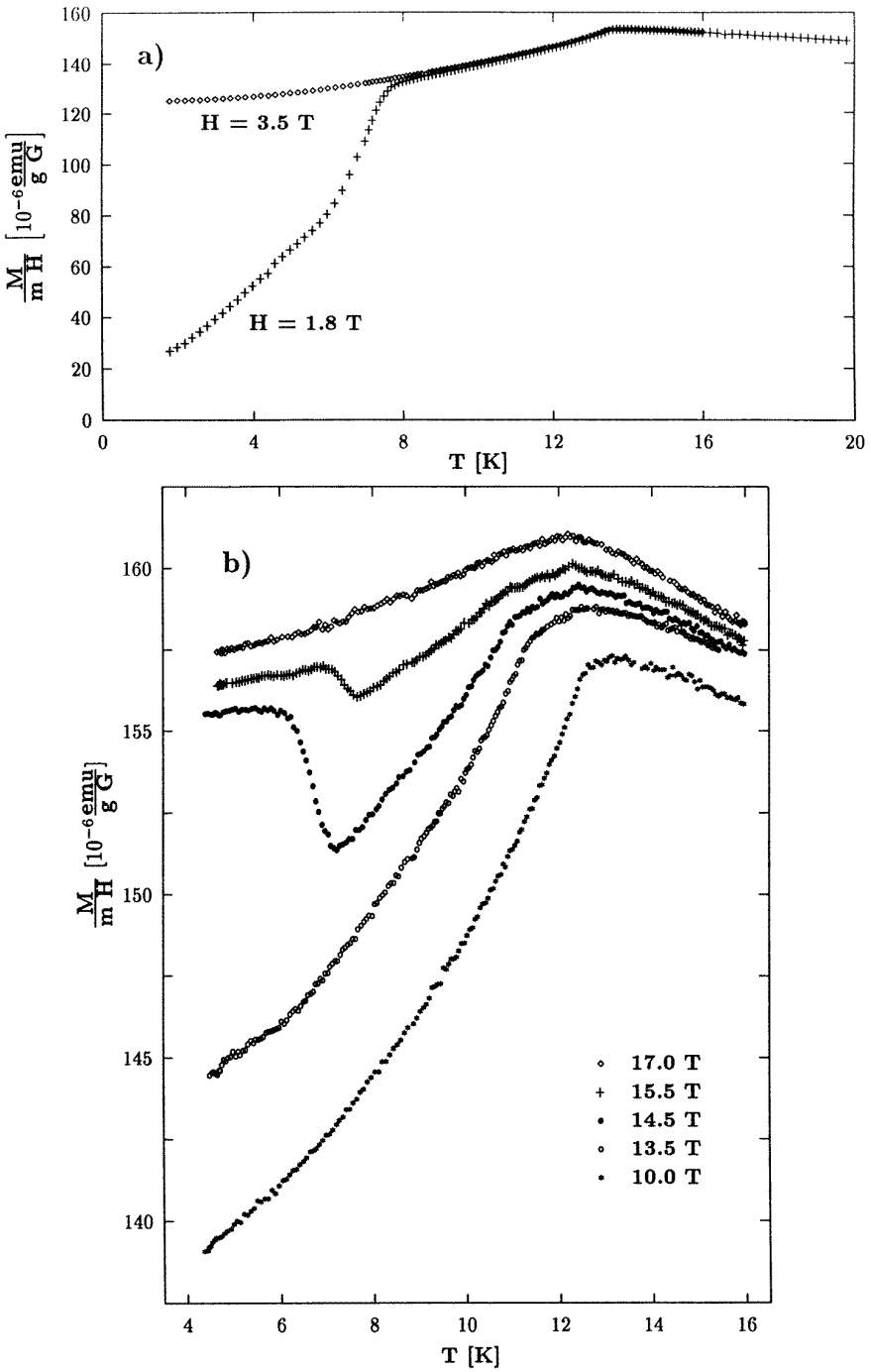

Figure 8. The temperature dependence of the magnetization for external fields parallel to the easy direction at constant field strengths (a) of $H = 1.8$ T and 3.5 T, measured using a superconducting quantum interference device from Quantum Design and (b) from $H = 10.0$ T to 17.0 T, measured using an extraction magnetometer in a resistive magnet at the Grenoble High Magnetic Field Laboratory.

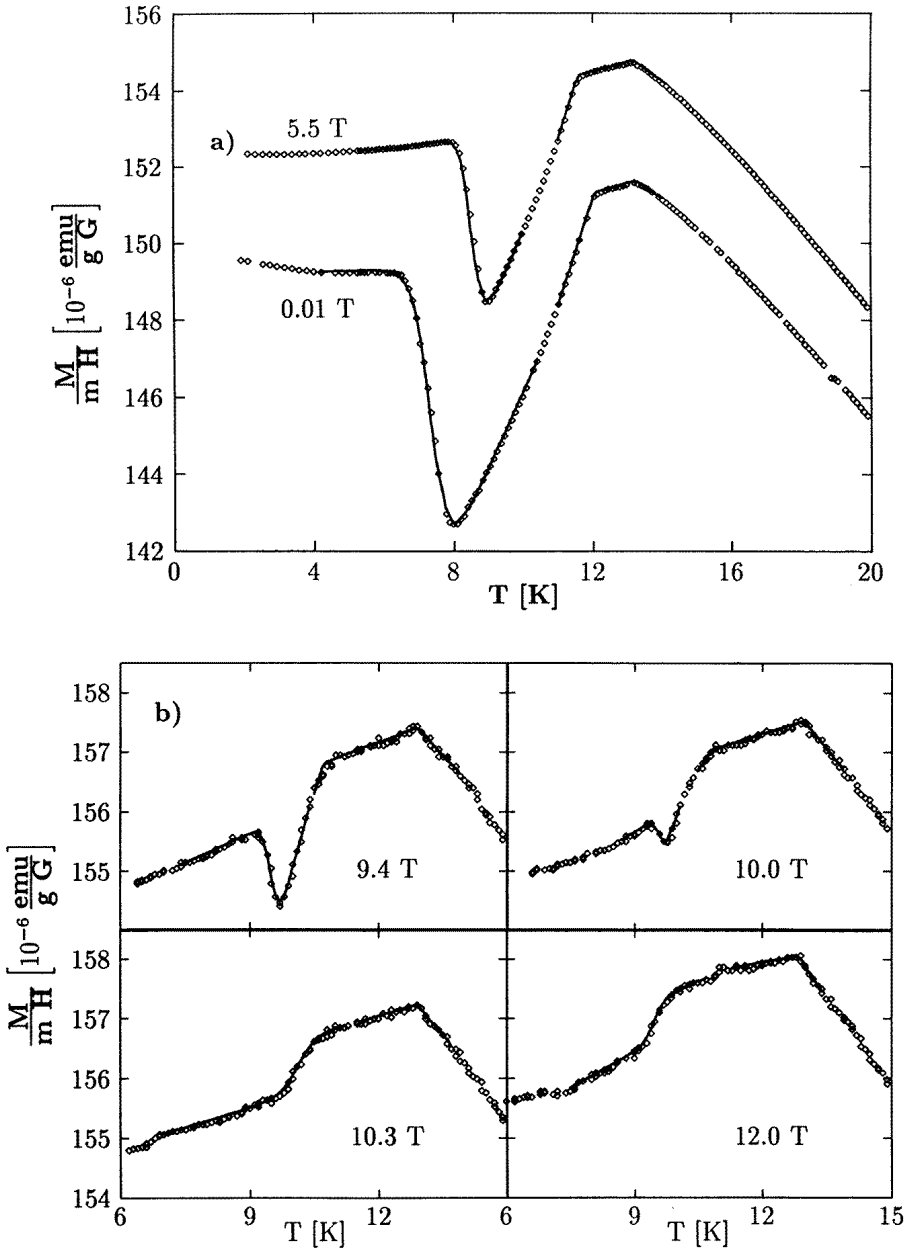

Figure 9. The temperature dependence of the magnetization for external fields parallel to [010] at constant field strengths (a) of $H = 0.01$ T and 5.5 T, measured using a superconducting quantum interference device from Quantum Design and (b) from $H = 9.4$ T to 12.0 T, measured using a vibrating-sample magnetometer from Oxford Instruments.

temperatures the magnetic field is applied in the direction of the ordered magnetic moments in the AF1 phase, and with decreasing temperature the magnetization goes to zero. On the other hand, for increasing temperature the phase transition AF1 $\rightarrow$ AF2 results in a

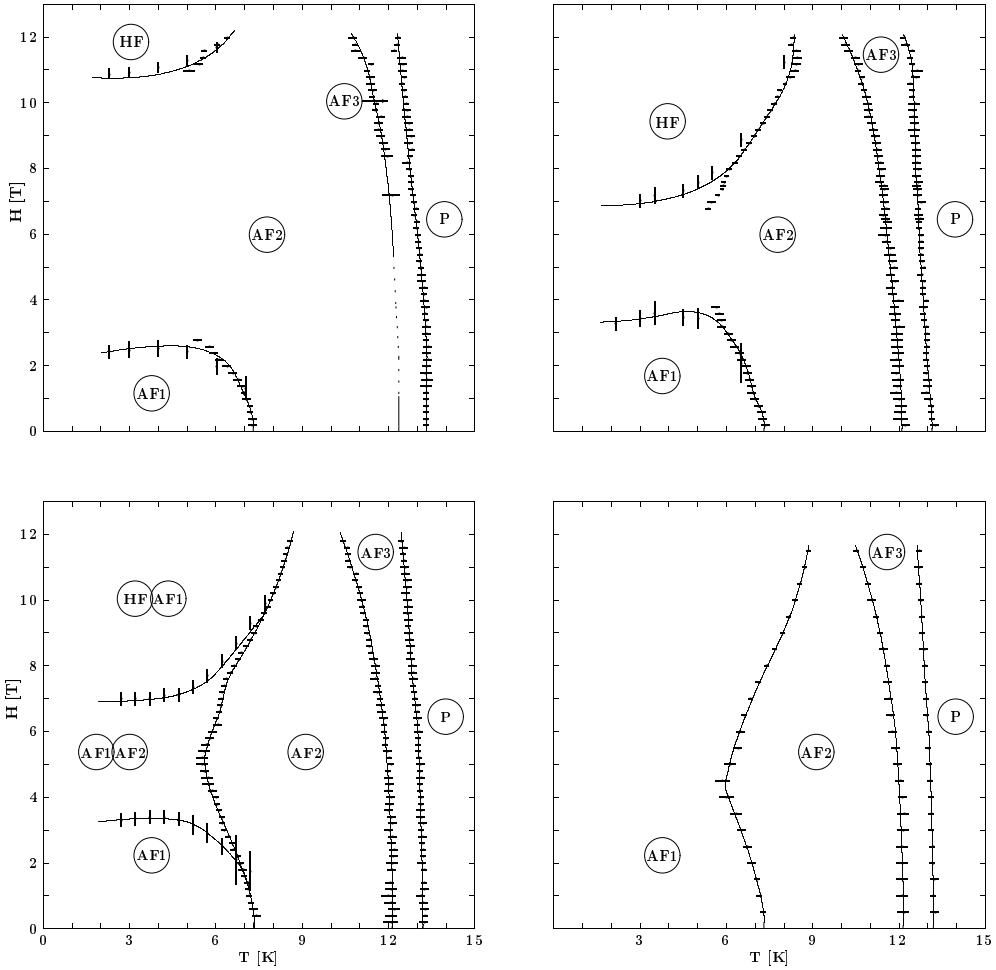

Figure 10. The magnetic phase diagrams of $MnWO_4$ for applied fields in the plane spanned by the easy direction and [010] for different values of φ, i.e. the angle formed with the easy direction: $\varphi = 30^\circ$ (top left), $\varphi = 45^\circ$ (top right), $\varphi = 47.5^\circ$ (bottom left) and $\varphi = 50^\circ$ (bottom right).

jump of magnetization $\Delta M > 0$. At higher temperatures the bends in the magnetization indicate the phase transitions AF2 $\rightarrow$ AF3 and AF3 $\rightarrow$ the paramagnetic region P. For a field strength $H > 2$ T the situation is different in the low-temperature region, because the phase AF2 is stabilized to the lowest temperatures examined, so the magnetic field is not applied in the direction of the ordered moments any longer, and therefore the magnetization does not go to zero if extrapolated to $T = 0$ K. At higher field strengths the transitions HF $\rightarrow$ AF2 $\rightarrow$ HF are indicated by the pronounced minimum in the temperature dependence of the magnetization for $H = 14.5$ T and 15.5 T; see figure 8(b).

The phase diagram for this field direction up to $H = 5.5$ T was first determined in a preliminary study for this contribution [2]. In this reference the phase AF2 was identified at $T = 1.8$ K and $H = 3.8$ T by a complete structure determination using single-crystal neutron diffraction.

Another field direction of particular interest is [010], not only pronounced by the monoclinic symmetry, but also, in particular, by the additional component of the ordered magnetic moment in this direction, which exists only in the AF2 phase but vanishes in the AF1 and AF3 phases.

4.2. The external field parallel to [010]

The phase diagram for this direction is shown in figure 11—see later—and can be derived from magnetization studies alone. The temperature dependence of the magnetization is illustrated in figure 9 for different field strengths. With respect to the phase transitions at $H = 100$ G the stability range of the AF2 phase is significantly reduced at $H = 5.5$ T while both phases AF1 and AF3 are stabilized by an external magnetic field applied in this direction. This tendency continues with a further increase of field strength, and the AF2 phase vanishes at $H = 10.2$ T, revealing a phase transition AF1 $\rightarrow$ AF3 with $\Delta M > 0$ for higher field strength, rather than $\Delta M < 0$ which was obtained for the transition AF1 $\rightarrow$ AF2.

4.3. The external field in the plane spanned by the easy direction and [010]

The specific orientation of an external field within this plane is uniquely determined by the angle φ formed with the easy direction. In this notation, the field direction in section 4.1 corresponds to $\varphi = 0^\circ$ and that in section 4.2 to $\varphi = 90^\circ$. To study the metamorphism between the different topologies of the diagrams for $\varphi = 0^\circ$ and $\varphi = 90^\circ$, experiments were performed at several intermediate field directions, summarized in the diagrams of figures 10 and 11. For the direction $\varphi = 30^\circ$ the phase AF3 is slightly stabilized for higher fields and no longer vanishes for the field strength under consideration. The high-field phase HF is observed at much lower fields of 11 T as compared to 14 T for the easy direction. In contrast, the field-induced transition AF1 $\rightarrow$ AF2 takes place at higher field strength. This shift of phase boundaries continues with increasing values of φ up to $\varphi = 45^\circ$. Varying φ from $\varphi = 90^\circ$ to $\varphi = 50^\circ$ does not change the topology of the phase diagram; only the field strength at which AF2 vanishes is shifted to higher fields. For the intermediate direction of $\varphi = 47.5^\circ$ the phase transitions for the topologies with $\varphi = 45^\circ$ and $\varphi = 50^\circ$ are simultaneously observed. This is a consequence of the crystal mosaicity of 1° and an estimated inhomogeneity in the applied field of the same magnitude. Therefore the local field directions in the antiferromagnetic domains differ, and some parts of the crystal respond accordingly to the $\varphi = 50^\circ$ phase diagram and other parts to that for $\varphi = 45^\circ$. The topology of both diagrams changes abruptly with the variation of φ at $\varphi_0 = 47.5(2.0)^\circ$.

4.4. The external field perpendicular to the easy direction and [010]

For the sake of completeness, additional experiments were performed with an external magnetic field perpendicular to the plane spanned by the easy direction and [010]. As shown in figure 12, the stability ranges of the phases AF1, AF2 and AF3 are hardly affected by the external field for this case.

5. Discussion

In zero field the magnetic ordering in $MnWO_4$ takes place with two intermediate phases AF2 and AF3, which are only stable over a small temperature range just below the Néel

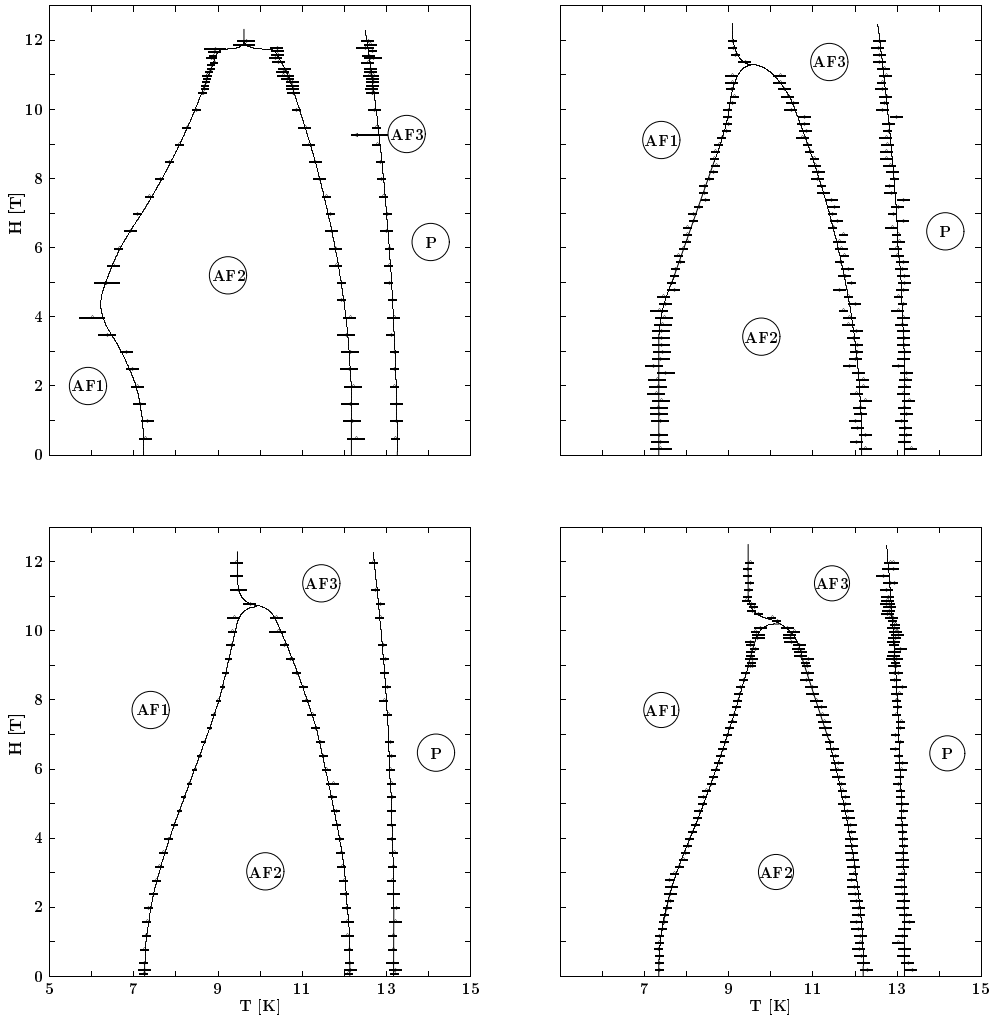

Figure 11. As figure 10, but for $\varphi = 52.5^\circ$ (top left), $\varphi = 60^\circ$ (top right), $\varphi = 75^\circ$ (bottom left) and $\varphi = 90^\circ$ (bottom right).

temperature. These long-periodic or incommensurate structures lock into a smaller or commensurate cell via the transition to the AF1 phase. The intermediate phase AF2 recurs even at the lowest temperatures examined, if an external field parallel to the easy direction of AF1 is applied. This field-induced phase transition AF1 $\rightarrow$ AF2 can be denoted as a *pseudo-spin-flop transition*: on the one hand, the magnetic moments partially switch into the plane perpendicular to the applied field, because the AF2 phase has an additional component of the ordered magnetic moment in the [010] direction—this is typical for a spin-flop transition; on the other hand, the translation symmetry changes during this transition, which is typical for a spin-flip transition. With further increasing field strength, another first-order phase transition, AF2 $\rightarrow$ HF, takes place. Up to now, no neutron diffraction experiments have been performed on the high-field phase HF, but from the abrupt disappearance of the AF2 and HF phases with variation of the field direction at $\varphi_0 = 47.5(2.0)^\circ$, the same translation symmetry for both phases, HF and AF1, is suggested.

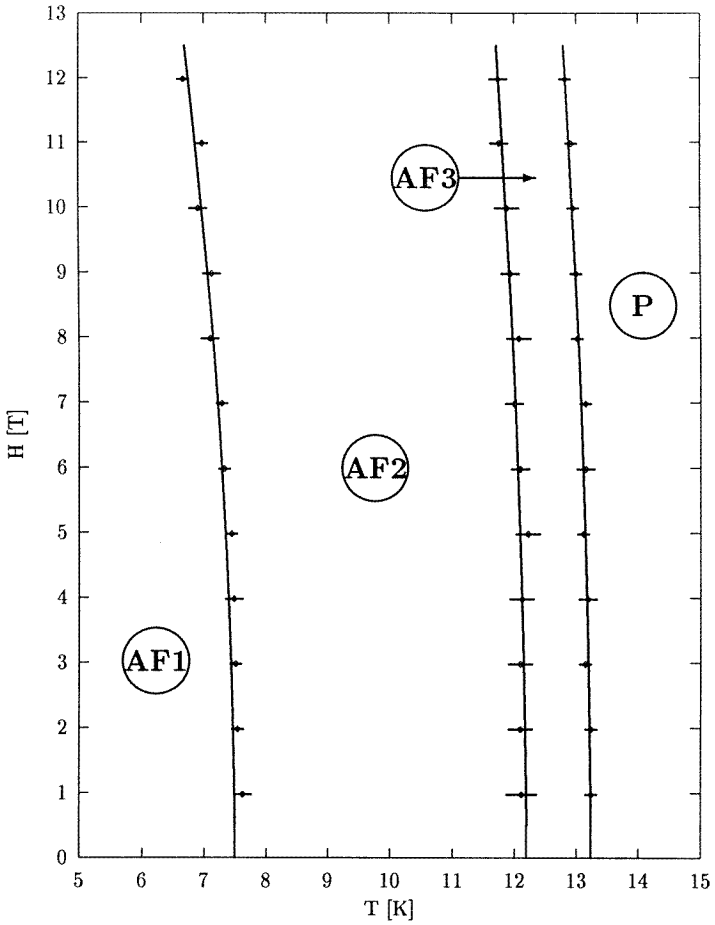

Figure 12. The magnetic phase diagram of $MnWO_4$ for an applied field perpendicular to the easy direction and [010].

A discussion of commensurate and long-periodic structures for the AF2 and AF3 phases versus incommensurability was given previously [1], but the more precise redetermination of the propagation vector $\boldsymbol{k}$ given in equation (1) leads to a slightly different commensurate indexing:

$$k_x = \frac{3}{14} \qquad k_y = \frac{1}{2} \qquad k_z = \frac{11}{24} \tag{4}$$

and therefore to a magnetic unit cell built up from $14 \times 2 \times 24$ crystallographic cells. No additional magnetic satellites with numerators other than 3 for k_x and 11 for k_z have been observed; such additional satellites would have indicated a commensurate model. For the case of incommensurability, the propagation vector $\boldsymbol{k}$ for the AF2 and AF3 phases should depend on an external parameter like temperature or field, which has also not been observed. The stability ranges of the AF2 and AF3 phases in zero field might be too small to detect a significant change of $\boldsymbol{k}$, and therefore neutron diffraction studies in high magnetic fields up to the field-induced transition AF2 $\rightarrow$ HF are needed for both the determination of the magnetic structure of HF and to resolve the question of commensurability or incommensurability

of the AF2 and AF3 phases. If the AF2 phase is incommensurate and the HF phase commensurate, a Lifshitz point exists at $T \approx 12$ K for an applied field $H \approx 14$ T parallel to the easy direction. If the AF2 and HF phases are both commensurate, a bicritical point exists at these values. For an applied field parallel to [010], all of the phases observed in zero field, AF1, AF2 and AF3, seem to form a triple point at $T \approx 10$ K and $H \approx 10$ T.

Acknowledgment

Support from the Bundesminister für Bildung und Forschung (grants No 03-FU3DAR and No 03-WE4DAR5) is gratefully acknowledged.

References

[1] Lautenschläger G, Weitzel H, Vogt T, Hock R, Böhm A, Bonnet M and Fuess H 1993 *Phys. Rev.* B **48** 6087
[2] Lautenschläger G, Weitzel H, Hock R and Burlet P 1994 *Institut Laue–Langevin, Grenoble, France, Annual Report 1993* p 53
[3] Ahrens R 1990 *Thesis* University of Karlsruhe, Germany